Forest Ecology and Management 549 (2023) 121475

Contents lists available at ScienceDirect

Forest Ecology and Management

journal homepage: www.elsevier.com/locate/foreco

Remotely sensed and ground measurements reveal intraspecific differences in early season needle unfolding and senescence, but lack of variability in litter flammability of *Pinus halepensis*

Erica Lombardi [a,b,*], Shawn Carlisle Kefauver [a,c], Luis Serrano [b], Ester Sin [b], Paula Piñas-Bonilla [d], Beatriz Pérez [d], Belén Luna [d], Gonzalo Zavala [d], Víctor Resco de Dios [a,b], Jordi Voltas [a,b]

[a] Joint Research Unit CTFC – AGROTECNIO – CERCA, Av. Alcalde Rovira Roure 191, Lleida 25198, Spain
[b] Departament of Agricultural and Forest Sciences and Engineering, Av. Alcalde Rovira Roure 191, Lleida 25198, Spain
[c] Integrative Crop Ecophysiology Group, Plant Physiology Section, Faculty of Biology, University of Barcelona, Av. Diagonal 643, 08028 Barcelona, Spain
[d] Department of Environmental Sciences, University of Castilla-La Mancha, Av. Carlos III, 45071 Toledo, Spain

ARTICLE INFO

Keywords:
Aleppo pine
Vegetation indexes
Intraspecific variability
Litter flammability
Needle phenology
Remote sensing

ABSTRACT

Pinus halepensis Mill. is a conifer typical of Mediterranean pinewoods adapted to drought and fire. Although the timing of seasonal events in *P. halepensis* is strongly associated with these stressors and other environmental factors, needle phenology and litter flammability are insufficiently characterized at the intraspecific level. These traits can be informative of the existence of locally adapted populations across the species' distribution range, and remote sensing approaches are promising tools to infer phenological changes in forest trees. In this study, we investigated intraspecific differentiation of *P. halepensis* related to needle phenology at the onset of the fire season (May-June) through vegetation indexes (VIs) obtained from unmanned aerial vehicles. We collected drone images using multispectral and RGB sensors for 56 adult populations of *P. halepensis* categorized into five ecotypes growing in two common gardens located in Spain under contrasting conditions (dry-continental *versus* wet-coastal). In the dry trial, we additionally monitored the temporal variation of RGB-derived indexes using two flights spaced over a one-month period. We also performed four consecutive ground measurements of needle pigments and fuel moisture content and obtained litter flammability traits for a subset of populations. Most *in situ* measurements and flammability traits did not show population differentiation. Regarding RGB-derived VIs, we did not detect obvious temporal patterns which differed among populations. However, we observed greener canopies in June than in May, which are indicative of the pace of current-year needle development. We also deduced an earlier phenology (i.e., earlier current-year needle unfolding) in the dry-continental trial. Ecotypic differentiation was found for some vegetation indexes related to needle unfolding (i.e., *TCARI/OSAVI*) and old needle senescence (i.e., *PRSI*). These differences were generally consistent across trials and time, and fundamentally indicated that sub-humid ecotypes typical of the eastern Mediterranean showed earlier needle unfolding and old needle senescence than semiarid ecotypes thriving in western continental Mediterranean areas. The intraspecific divergence observed in early season phenology is potentially related to the existence of contrasting life-history strategies present at the intraspecific level for the species. In particular, some semi-arid ecotypes, which are known to optimize the trade-off between carbon gain and water loss, exhibited an early old needle senescence (high likelihood of crown fire development) coupled with a late needle unfolding (conservative water use). These results indicate a possible trade-off between drought and fire resistance for the species, which suggest the importance of considering the intraspecific characteristics of Aleppo pine in forest management actions.

* Corresponding author at: Av. Alcalde Rovira Roure 191, Lleida 25198, Spain.
E-mail address: erica.lombardi@udl.cat (E. Lombardi).

https://doi.org/10.1016/j.foreco.2023.121475
Received 23 June 2023; Received in revised form 29 September 2023; Accepted 1 October 2023
Available online 12 October 2023
0378-1127/© 2023 The Author(s). Published by Elsevier B.V. This is an open access article under the CC BY license (http://creativecommons.org/licenses/by/4.0/).

1. Introduction

Pinus halepensis Mill. (Aleppo pine) is one of the most widespread conifers in the Mediterranean basin (Picornell-Gelabert et al., 2021; Mauri et al., 2016). It presents high economic and ecological value (Chambel et al., 2013) and, as such, it is widely used in reforestation programs of Mediterranean ecosystems (Taïbi et al., 2014). The species is resistant to drought and prevails in fire-prone habitats due to its adaptive strategies to cope with fire, including serotiny, poor apical dominance and profuse branching (Pausas, 2015). Owing to its high intraspecific variability and plasticity (Voltas et al., 2018), *P. halepensis* inhabits very contrasting ecological niches. The species thrives in very different soil types and can be found in most bioclimates of the Mediterranean region, with mean monthly minimum temperatures ranging from −2°C to 10 °C and mean annual precipitation varying between 350 and 1500 mm (Fady et al., 2003). Population differentiation has been widely studied for functional traits related to roots (Lombardi et al., 2021), crown structure (Lombardi et al., 2022), water use patterns (Voltas et al., 2015) and phenology (Klein et al., 2013), and also for remotely sensed vegetation indexes related to photosynthetic pigments, leaf area and water content (Santini et al., 2019b). On the contrary, knowledge on genetic variation in needle phenology is scarce (Santini et al., 2019b), and also on differentiation in flammability-related traits, which are widely studied at the interspecific level (Varner et al., 2022) but poorly investigated at the intraspecific level (Bastien & Ganteaume, 2020).

Understanding variation in the response of trees to disturbances has been a long-term goal of plant ecology (Grime, 1977). Some studies postulate that there is a fundamental trade-off between adaptations to drought and fire in pines (Karavani et al., 2018). It has been hypothesized that intraspecific variation in traits enhancing survival under drought occurs at the expense of increasing fire danger and, vice versa, that traits enhancing survival under fire may decrease performance under drought. For example, *P. pinaster* individuals with thick barks, which may better survive surface fires, tend to show reduced tolerance to embolism (Resco de Dios et al., 2018). A typical response in *P. halepensis* is to induce senescence in old needles at the beginning of the fire season (late spring), which diminishes transpiration area and, consequently, water demand, but at the potential expense of increasing flammability by decreasing fuel moisture content in the crown. However, most evidence for a trade-off between drought tolerance and fire resistance is anecdotal and lacking rigorous testing.

Phenology is a key driver of plant carbon and water cycles, and it can be defined as the timing of reproduction and of other events related to e.g., growth or senescence (Ye et al., 2023; Berra et al., 2019). The phenology of conifers comprises three main phases (bud dormancy, bud flush and needle senescence). Needle phenology in particular can be divided into unfolding, maturation, and senescence and fall (Kumar et al., 2019), and it involves changes in photosynthetic pigments and nutrient pools dynamics (Fréchette et al., 2020; Springer et al., 2017). Needle phenology is strongly correlated with environmental conditions, especially temperature and water availability (Peaucelle et al., 2019). It can influence fire behaviour by affecting live vegetation moisture, fuel vegetation structure or litter composition (Loudermilk et al., 2022; Silvério et al., 2015), and vice versa, fire can shape the composition and dynamics of forest ecosystems and thus affect tree phenology (e.g., timing of dormancy, growth and reproduction) (Miller et al., 2019; Risberg & Granström, 2009). Although field observations provide precise and important information on phenology, they are time-consuming and labour-intensive (Ciocîrlan et al., 2022). Lately, remote sensing is being used to effectively monitor tree phenology (Motohka et al., 2010), since images derived from satellites and, especially, from unmanned aerial vehicles (UAVs) can provide information at different spatiotemporal scales with high spatial resolution (Wong et al., 2020; Berra et al., 2019). In particular, multispectral and RGB (Red, Green and Blue) sensors mounted on UAVs detect light reflectance variation, potentially providing reliable phenological data at the individual level (Kleinsmann et al., 2023; Santini et al., 2019b).

A vegetation index (VI) is a simple mathematical calculation that integrates two or more wavelengths of spectral reflectance image data (spectral bands or images) for the assessment (estimation or enhanced visualization) of surface biophysical properties (Huete, 2012). To date, hundreds of vegetation indexes have been evaluated from both visible and non-visible (including near infrared, short-wave infrared and even thermal infrared) wavelengths. VIs can provide information about chemical and pigment leaf composition, water content, leaf area, canopy cover and canopy health, for instance (Ciocîrlan et al., 2022; Santini et al., 2019b; Xue & Su 2017; Stimson et al., 2005). VIs have been used widely in field crops research (Starý et al., 2020; Gracia-Romero et al., 2018), and also in forestry to estimate canopy properties at the stand or landscape levels (Wong et al., 2019; Klosterman et al., 2018). Currently, many VIs are used to infer plant phenology, both multispectral-derived (especially those using the reflectance in the near-infrared region) and RGB-derived indexes. Tree level, RGB-derived indexes can be considered an affordable alternative to multispectral records if acquired through UAVs (Starý et al., 2020; Gracia-Romero et al., 2018; Kefauver et al., 2015). However, applications of VIs to assess crown properties and tree phenology at the intraspecific level are still scarce, especially for evergreen conifers (Ciocîrlan et al., 2022; Wong et al., 2022; Santini et al., 2019b).

In this study, we used VIs obtained from UAVs along with field samples collected *in situ* to identify intraspecific differences in needle phenology of *P. halepensis*. We were particularly interested in characterizing needle unfolding and old needle senescence at the onset of the wildfire season in the western Mediterranean (end of spring). Needle lifespan in *P. halepensis* is approximately-three years, and three-years-old needles usually become dry and senesce towards the second half of June. Moreover, we evaluated intraspecific variation of litter flammability and other flammability traits such as live fuel moisture content (*FMC*). We used two common garden experiments characterised by a dry, continental climate (Zuera, north-eastern Spain), and a coastal, subhumid Mediterranean climate (Altura, eastern Spain). By using range-wide populations, we sought to describe intraspecific genetic variation in needle phenology related to photosynthetic pigments at the onset of the fire season (May-June), which can be potentially informative of differential plasticity and adaptation to varying conditions across the Mediterranean basin.

We expected an earlier phenology in the inland site as a consequence of drier conditions for the species related to higher temperatures and less available water, as previously described for needle unfolding (Camarero et al., 2022). We hypothesized that differences among populations for both *in situ* traits and RGB and multispectral indexes would reflect different phenological responses (i.e., needle unfolding, old needle senescence) during late spring. In this regard, we also expected to detect intraspecific differences for flammability traits potentially related to contrasting evolutionary histories in fire-prone habitats. Specifically, we presumed that populations and ecotypes experiencing less water availability at their origin could show less *FMC*, earlier old needle senescence and delayed needle unfolding as a result of a more conservative water-use strategy. Because of their higher tolerance to drought, these populations may have less survival chances under surface and crown fires due to trade-offs among plant functional traits (i.e., enhanced flammability) (Karavani et al., 2018; Resco de Dios et al., 2018).

2. Material and methods

2.1. Study sites

The study was performed in two common gardens (provenance trials) located in Zuera (Zaragoza province, Spain; 41°52′24"N, 00°38′57"W, 425 m a.s.l.) and Altura (Castellón province, Spain; 39°49′29"N, 00°34′22"W, 640 m a.s.l.) (Fig. 1). Zuera and Altura hold

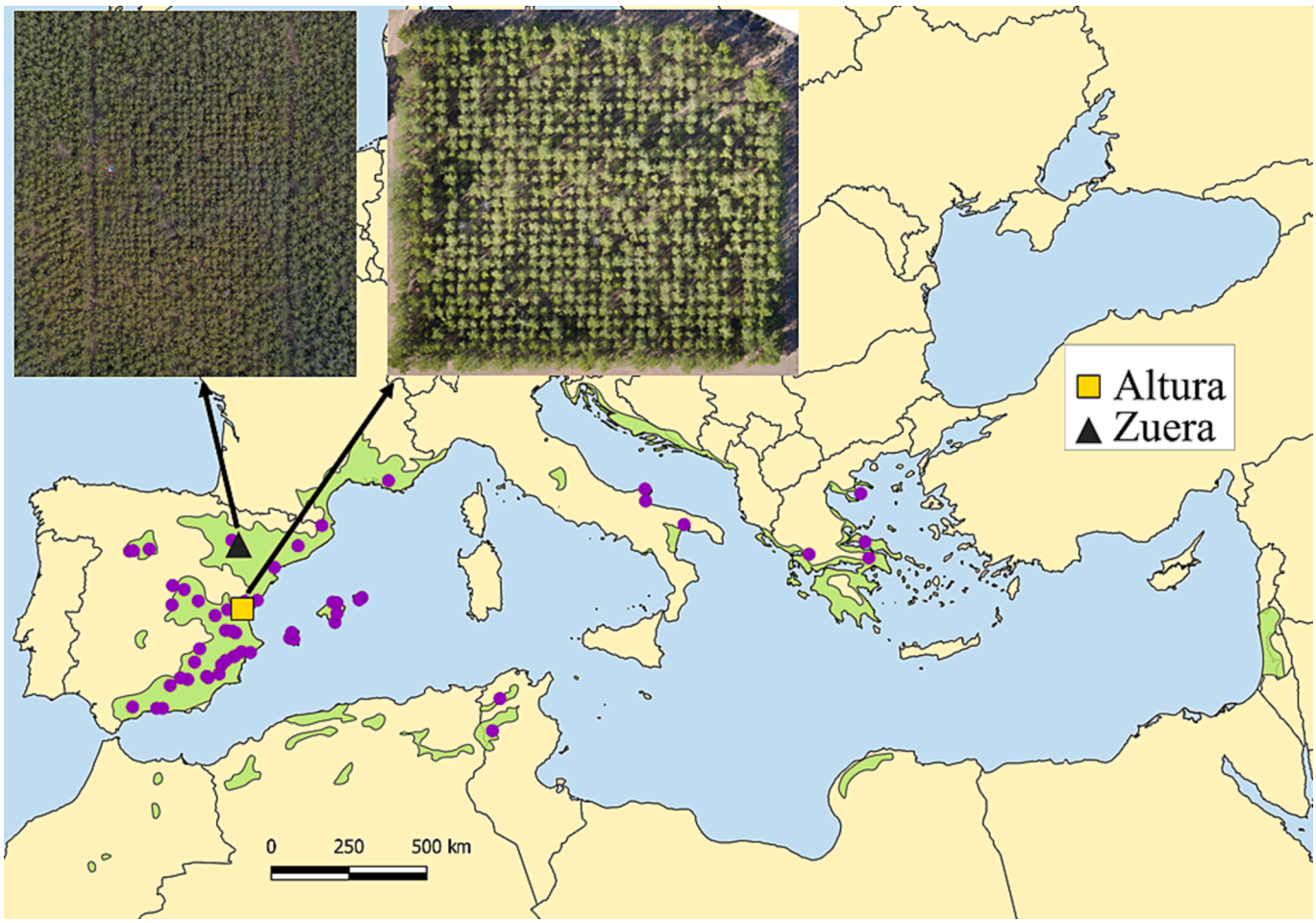


Fig. 1. Geographic origin of 56 Pinus halepensis populations (purple dots), evaluated in two common gardens experiments used in this study: Altura (Castellón province, Spain) and Zuera (Zaragoza province, Spain). The green area represents the natural distribution of *P. halepensis* according to EUFORGEN (http://www.euforgen.org/species).

721 (80 % survival) and 807 (90 % survival) adult trees respectively. These trees belong to 56 populations of *P. halepensis* originating from mainland Spain, Balearic Islands, France, Greece, Italy and Tunisia (Table S1). The seeds were collected in 1995 from 20 to 30 adult individuals per population, spaced at least 100 m apart, and were sown in a forest nursery in Spain using standard container practices (Landis, 1990) the following year. In 1997, 896 one-year old seedlings (16 seedlings per population) were transplanted at both study sites. The experimental design was a Latinised row-column with four replicated blocks (John & Williams, 1998). This design efficiently controls intra-site variability, as systematic changes in both column and row directions can be incorporated into linear mixed-effects models.

We used all trees available in both trials for obtaining UAV-based data, while a subset of trees from Zuera (a total of 36 individuals belonging to six populations) was used for ground truthing. This subset contained populations from the Iberian Peninsula, Balearic Islands, Tunisia and Greece as representative of most current distribution range of the species. Aleppo pine populations were further grouped into five climate-based ecotypes, as proposed by Patsiou et al. (2020): dry-summer/semiarid/temperate (DST), dry-summer/semiarid/cold (DSC), dry-summer/sub-humid/temperate (DHT), wet-summer/semiarid/temperate (WST), and wet-summer/sub-humid/cool (WHC). This division stemmed from a hierarchical cluster analysis based on climatic information of populations for the purpose of delineating broad intraspecific patterns of growth performance under different climate change scenarios (Patsiou et al., 2020).

2.2. Plant material and climate data

We collected needles of six populations (#11, 142, 152, 182, 214 and 242; Table S1) during four sampling campaigns in 2021 (May 14th and 28th, June 11th and July 2nd). Needles were obtained from healthy mid-canopy branches of six trees per population following the column direction of the trial. These branches were accessible with a telescopic lopper, while the sparse foliage of Aleppo pine made possible that full sunlight reached most of its crown. Two to five branchlets were sampled per tree (Minocha et al., 2009). Aleppo pine generally starts to develop new needles in spring, and these needles can be retained in the tree for three years before senescing (Balaguer-Romano et al., 2020; Girard et al., 2011). The sampled needles corresponded to the previous year cohort (1-yr old) or to older cohorts (≥2-yr old), since current year needles were just emerging and not clearly visible in the two earlier sampling campaigns. Needle tissue was used to quantify chlorophyll content (*Chl*), particularly chlorophyll a (Chl_a), chlorophyll b (Chl_b) and total chlorophyll (Chl_{a+b}), total carotenoid content (*Car*) and live fuel moisture content (*FMC*). We collected additional needles during the last sampling campaign to infer specific leaf area (*SLA*) and stomatal conductance (*GSW*).

The needles used to determine *Chl* and *Car* were immediately frozen in the field and stored in a dark place. *Chl* and *Car* were measured following the protocol by Minocha et al. (2009). We chopped 15 mg of unfrozen samples into 1.5 ml of 95 % ethanol and afterwards they were stored in a water bath at 65 °C for 16 h. Once the samples were removed from the water bath, they were left few minutes at room temperature to

equilibrate, and then vortexed for 1 min at low speed. Finally, the samples were centrifuged for 5 min at 13,500 g. We then recorded the absorbance at 649 nm, 664 nm and 470 nm using a UV spectrophotometer (UV-1600 PC, VWR International, Belgium). Chl_a, Chl_b, Chl_{a+b} and *Car* were estimated using the following equations:

$$\text{Chla} = (13.36 \times \text{A664}) - (5.19 \times \text{A649}) \quad (1)$$

$$\text{Chlb} = (27.43 \times \text{A649}) - (8.12 \times \text{A664}) \quad (2)$$

$$\text{Chla} + \text{b} = \text{Chla} + \text{Chlb} \quad (3)$$

$$\text{Car} = (1000 \times \text{A470} - 2.13 \times \text{Chla} - 97.46 \times \text{Chlb}) / 209 \quad (4)$$

The needle samples used to estimate *FMC* were stored in metallic tins sealed with parafilm. Once in the laboratory we weighted the fresh weight of samples, which were then oven-dried at 105 ℃ during 48 h (Matthews, 2010). Afterwards the samples were weighted again, and *FMC* was calculated as follows:

$$\text{FMC} = \frac{\text{FW} - \text{DW}}{\text{DW}} \times 100 \quad (5)$$

where *FW* represents the fresh weight (g) and *DW* is the dry weight (g).

Leaf area (*LA*) was estimated using a scanner Area Meter (AM100, ADC, UK) using ten needles per population. After that, the samples were oven-dried at 105 ℃ during 48 h (Matthews, 2010) to obtain leaf dry weight (*DW*), and *SLA* was calculated as:

$$\text{SLA} = \frac{\text{LA}}{\text{DW}} \quad (6)$$

Stomatal conductance was measured in the field using a LI-600 porometer (LI-COR Biosciences, Lincoln, NE, USA). We placed the needles in a plane across the leaf chamber aperture and we covered the side in contact with the atmosphere to avoid air leakage and ensure a stable reading for every measurement. We made three measurements per tree and their average was used for statistical analysis.

For each population, climate data at origin was obtained from the WorldClim database (Fick, 2017) at 1 km^2 spatial resolution. We used the complete set of 19 bioclimatic variables available in the database.

2.3. UAV-based flights and images processing

For the Zuera trial, RGB images were acquired through a UAV Mavic 2 Pro (DJI, China) equipped with a RGB integrated 20 MP camera, while multispectral images were acquired through a UAV Oktokopter 6S12 XL (Mikrokopter, Germany) equipped with a micro-MCA 11 + ILS (Incident Light Sensor for dedicated band-wise spectral calibration) multispectral camera (Tetracam Inc., Chatsworth, CA, USA). The multispectral camera had 11 bands (the specific wavelengths captured by the sensor are described in Table S2). Two consecutive flights, each performed with UAV Mavic and UAV Oktokopter, were done at around midday on May 14th and on June 11th (2021) at an altitude of 57 m. A total of 385 images were obtained with the RGB camera, while 105 images were acquired with the micro-MCA camera. A field spectrometer ASD FieldSpec Pro FR^{TM} (USA) was used to measure, *a posteriori*, the absolute reflectance of the multi-colour landing panels in optimal light conditions and, hence, to provide a secondary empirical calibration to the micro-MCA data. Measurements made with the field spectrometer were employed to improve the instantaneous spectral calibration of the micro-MCA camera as flying conditions were sub-optimal, with some light cirrus clouds and moderate to heavy winds.

For the Altura trial, RGB and multispectral images were acquired on May 25th (2017) using the same Oktokopter 6S12 UAV described above for Zuera. A Lumix GX7 RGB camera (Panasonic, Japan) with a 20 mm focal length and 16 MP resolution was used for the acquisition of RGB images, while a micro-MCA 12 + ILS multispectral camera with 10 bands (Tetracam Inc., Chatsworth, CA, USA) and 15.6 MP resolution (1.3 MP for each of 12 sensors) was employed to capture multispectral images (the wavelength capture by each sensor is described in Table S3). The ILS processing included in the Tetracam PixelWrench software includes all calibration steps to at-sensor reflectance, including parallax adjustments, DN and Dark Current.

2.4. Imagery processing

The Agisoft Metashape Professional software (Agisoft LLC, St. Petersburg, Russia, version 1.6.3.10732) was employed to align the multispectral or RGB images and produce dense points clouds and orthomosaic images. Spectral calibration was done using ENVI 5.6.3 (NV5 Geospatial Solutions, Broomfield, CO). Unfortunately, we could not use the multispectral data retrieved in Zuera on May 14th due to technical reasons regarding the spectral calibration.

We used the open-source software LAStools (version 201003) (Isenburg 2017) and US Forest Service FUSION/LDV (version 4.21) (McGaughey, 2015) to eliminate noisy points, classify the valid points and normalize the RGB point clouds (through *lasnoise*, *lasclassify* *lasheight* functions in LAStools), and also to obtain a digital terrain model (DTM) and a canopy height model (CHM) (through *GridSurfaceCreate* and *CanopyModel* functions in FUSION/LDV) (Lombardi et al., 2022). After that, we applied the *vwf* function (Popescu & Wynne, 2004) implemented in the ForestTools R package (version 4.1.2) (Plowright, 2018) to identify individual treetops. After visual inspection and manual correction of trees marked by the algorithm, we run the *mcws* function (Meyer & Beucher, 1990) of ForestTools to segment tree crowns, which were again visually inspected and manually corrected in QGIS (version 3.26.3). Afterwards, total tree height and crown area were estimated at the tree level. We did not validate tree height and crown area with ground-truth data; however, a validation procedure previously carried out in a twin common garden experiment to those of Zuera and Altura was highly satisfactory (R^2 of 0.8 and RMSE of 0.45 m) (Lombardi et al., 2022).

2.5. Multispectral and RGB vegetation indexes (VIs)

Vegetation indexes (VIs; Table 1) were calculated in QGIS through the raster calculator option for both the RGB and multispectral orthomosaics. Every index was calculated at the tree level (a workflow of the process is summarized in Fig. 2) using the zonal statistics function of QGIS. To this end, we used the average pixel value of each crown. We calculated four RGB-derived VIs: green percentage index (*G%*), green–red vegetation index (*GRVI**), green leaf index (*GLI*), and triangular green index (*TGI*). We also obtained six multispectral-derived VIs: normalized difference vegetation index (*NDVI*), plant senescence reflectance index (*PSRI*), green ratio vegetation index (*GRVI*), enhanced vegetation index (*EVI*), transformed chlorophyll absorption reflectance index (*TCARI*), and optimized soil adjusted vegetation index (*OSAVI*). We also calculated the ratio between the last two indexes (*TCARI/OSAVI*). Two additional multispectral VIs were also calculated in Zuera, the chlorophyll/carotenoid index (*CCI*) and the photochemical reflectance index (*PRI*), as the micro-MCA sensors partially changed between trial flights to improve the acquisition of vegetation information.

The two common gardens evaluated are free from understory. Thus, the reflected signal was unlikely affected by different backgrounds through time and among trial locations.

A brief description of the VIs used in this study is as follows. *G%* is one of the mostly used RGB VI to track plant phenology (Larrinaga and Brotons, 2019; Alberton et al., 2014; Sonnentag et al., 2012). It quantifies vegetation greenness through changes in leaf color (Alberton et al., 2014; Thapa et al., 2021). *GRVI** is sensitive to green color (Tucker, 1979) and it is also associated with leaf color changes (Motohka et al., 2010). It has been used in previous studies to monitor phenological changes (Anderson et al., 2016; Motohka et al., 2010). *GLI* is obtained using all three bands of the RGB camera (Louhaichi et al., 2001) and is

Table 1
RGB and multispectral-based vegetation indexes (VIs) used in this study. The calculation of VIs was based on reflectance (*R*) of particular wavelengths. The table shows the abbreviation of each index, the wavelengths involved, the formula applied and the appropriate reference. Where G = green colour channel (0–255); R = red colour channel (0–255); and B = blue colour channel (0–255). *G%* = green percentage index; *GRVI**= green–red vegetation index; *GLI* = green leaf index; *TGI* = triangular green index; *NDVI* = normalized difference vegetation index; *CCI* = chlorophyll/carotenoid index; *PRI* = photochemical reflectance index; *PSRI* = plant senescence reflectance index; *GRVI* = green ratio vegetation index; *EVI* = enhanced vegetation index; *TCARI* = transformed chlorophyll absorption reflectance index; *OSAVI* = optimized soil adjusted vegetation index.

	VI	Formula	References
RGB VIs	*G%*	G/(R + G + B)	Woebbecke et al., 1995
	*GRVI**	(G − R)/(G + R)	Tucker, 1979
	GLI	((G − R) + (G − B))/2G + R + B	Louhaichi et al., 2001
	TGI	−0.5 × [190 × (R − G) − 120 × (R − B)]	Hunt et al., 2011
Multispectral VIs	*NDVI*	$(R_{840} - R_{670})/(R_{840} - R_{670})$	Rouse et al., 1973
	CCI	$(R_{532} - R_{670})/(R_{532} + R_{670})$	Gamon et al., 2016
	PRI	$(R_{532} - R_{570})/(R_{532} + R_{570})$	Gamon et al., 1992
	PSRI	$(R_{670} - R_{570})/(R_{840})$	Merzlyak et al., 1999
	GRVI	R_{840}/R_{570}	Sripada et al., 2006
	EVI	$2.5 \times (R_{840} - R_{670})/[(R_{840} + 6 \times R_{670} - 7.5 \times R_{450}) + 1]$	Huete et al., 2002
	TCARI	$3 \times (R_{700} - R_{670}) - 0.2 \times (R_{700} - R_{570}) \times (R_{700}/R_{670})$	Haboudane et al., 2002
	OSAVI	$(1 + 0.16) \times (R_{840} - R_{670})/(R_{840} + R_{670} + 0.16)$	Rondeaux et al., 1996

sensitive to leaf chlorophyll content (Bulut, 2023). *TGI* is mostly associated with nitrogen and chlorophyll content (Hunt et al., 2011), and it has been used to detect changes in plant phenology (Starý et al., 2020, Hunt et al., 2012). *NDVI* is a commonly used VI calculated from the red and the near-infrared wavebands (Rouse et al., 1973) that has been used in many studies as a proxy for plant productivity and phenology (Wong et al., 2020; Santini et al., 2019b; Anderson et al., 2016). *PSRI* is also associated with photosynthetic pigments (Merzlyak et al., 1999) and has been used to monitor changes during leaf senescence (Li et al., 2022; Olmo et al., 2021). *GRVI* is sensitive to photosynthetic rates and can be used to estimate changes in leaf pigments (Sripada et al., 2006). *EVI* is considered an improved *NDVI* (Huete et al., 2002) that is less affected by atmospheric conditions and soil background. *TCARI* indicates leaf chlorophyll absorption (Haboudane et al., 2002) and it is often used in conjunction with *OSAVI* (Rondeaux et al., 1996) as a proxy for leaf area index (LAI) that minimizes soil background. Thus, *TCARI/OSAVI* can estimate leaf chlorophyll content independently of leaf area (Zarco-Tejada et al., 2004). *CCI* (Gamon et al., 2016) and *PRI* (Gamon et al., 1997) are sensitive to carotenoid and chlorophyll pigments, particularly to the ratio *Car* to *Chl*. These two indexes are associated to photosynthetic activity and can be considered proxies for photosynthetic phenology (Wong et al., 2020; Fréchette et al., 2016). Both are particularly suitable to monitor the phenology of photosynthesis in evergreen conifers (Wong et al., 2020; Springer et al., 2017).

To overcome noise caused by soil pixels contained into previously segmented single crowns, RGB and multispectral images were filtered as follows. For RGB images, negative values of *GRVI* were considered as soil pixels, since *GRVI* is also used to estimate biomass and green vegetation, with *GRVI* = 0 used as threshold (Chen et al., 2019; Motohka et al., 2010). For multispectral images, *NDVI* values were used by choosing a pixel threshold of 0.5, since *NDVI* values close to 0 represent barren rocks and soil whereas values above 0.5 indicate healthy vegetation (Sharma et al., 2022; Santini et al., 2019b).

2.6. Flammability experiment

Needle litter was collected in July 2022 in Zuera (about 100 g per

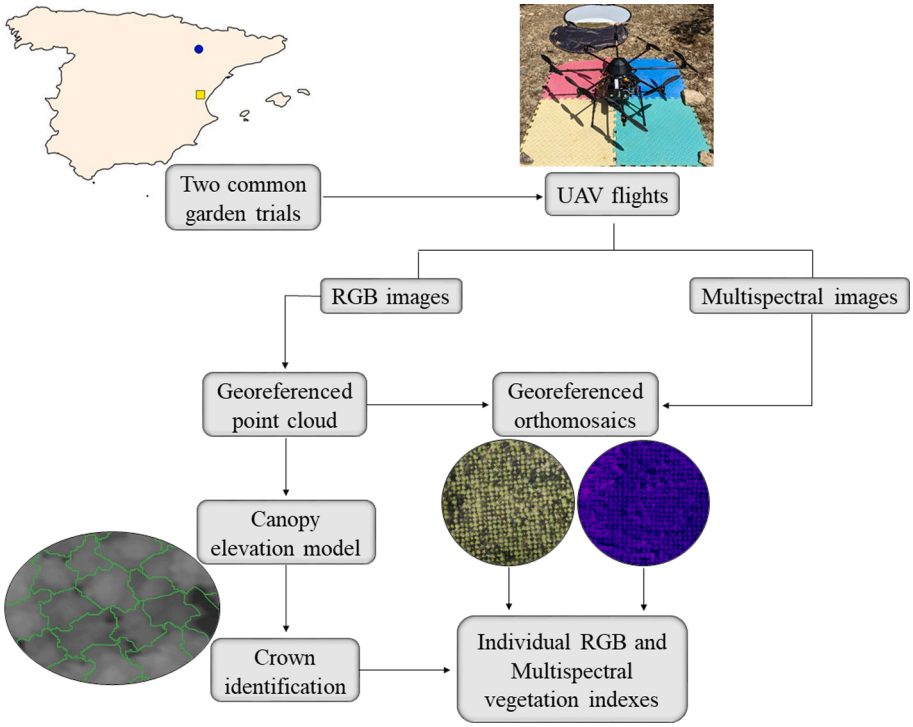


Fig 2. Flowchart summarizing the processing of RGB and multispectral images to obtain vegetation indexes at the tree level (i.e., phenotypic data).

sample) from ten populations and three blocks (two populations per ecotype, as follows: #11, 31, 142, 143, 152, 154, 182, 186, 214 and 242; Table S1). Only needle litter fallen between the two central trees of each experimental unit was collected to minimize contamination from adjacent units. Needle length was measured at the nearest millimeter using the open software ImageJ (version 1.52a) (Schneider et al., 2012). In order to equilibrate needle temperature and humidity we weighted 75 g per litter sample, which were later put in an oven at 30 ℃ for five days. Samples were removed from the oven one by one just before the experiment started in order to keep needle litter in equilibrium moisture content. As final checking, samples were re-weighed following the period in the oven. Their weight varied between 72 and 73 g, and their humidity (combustible humidity) ranged from 4.4 % to 7.6 %.

For the flammability experiment we followed established protocols (Varner et al., 2015, Fonda, 2001). The weighed litter samples were spread across a 20 × 20 cm grid with ethanol-soaked cotton strings placed on one side of the grid. Fuel bed depth was measured to the nearest mm in three different locations of each fuel bed. Fuel bed depth varied between 2.5 and 5 cm among samples. Two thermocouples were placed on top of each fuel bed approximately at 2 cm from each side, which recorded temperature every second, from which we obtained the mean peak heat (℃). Right after the cotton was ignited the fuel burnt immediately, and we calculated (1) the time elapsed until the flame arrived to the opposed side of the grid (diffusion flame time), (2) the time elapsed until the flame extinguished (flame time), and (3) the time elapsed until the last ember extinguished and the smoke stopped (smoldering combustion time). The maximum height reached by the flame (flame height) was visually estimated to the nearest cm by an observer using a ruler mounted behind the fire chamber. A camera model Nikon d5300 (Nikon Corp., Japan) was mounted on a tripod to record the entire experiment and double check the estimation of the maximum flame height and the remaining parameters if needed. The amount of fuel combusted was calculated as the proportion of the initial litter mass to the remaining mass, while the mean rate weight loss (*WL*) was estimated by dividing the lost weight by smoldering combustion time (Fonda, 2001). An example of the experimental protocol followed can be visualized in a video (available at www.kapwing.com/w/faCxHvtC86).

2.7. Statistical analyses

Population differentiation was first tested for each phenotypic trait measured *in situ*, independently for each of three field campaigns, through analysis of variance (ANOVA), with populations and replicates as fixed terms. One field campaign (June 11th) could not be analyzed independently due to large gaps in the dataset as a result of heavy rain preventing a complete collection of samples. Traits that had been measured across campaigns were then subjected to linear mixed-effects models with a repeated time structure in order to estimate the temporal effect and its variability among populations, taking also into account needle age as main factor in the models.

For RGB- and multispectral-derived VIs, ANOVAs were run independently for each trial to check for genetic variability among populations. In the case of Zuera, we used either (i) data acquired during the June flight, when both types of VIs (RGB and multispectral) were available, or (ii) RGB-derived data taken across flights, which were subjected to linear mixed-effects models with a repeated time structure for time-series analysis. In the latter case, this allowed to estimate temporal changes in VIs and its differential plasticity among populations. In all cases, the population effect was partitioned into an ecotype effect plus a population-nested-to-ecotype residual to evaluate the presence of a broad ecotypic structure in the dataset. Least significant difference tests (LSD) were used to statistically compare ecotype means.

Populations' means of VIs exhibiting significant population effects were correlated to climate at the origin of populations. Pearson's correlations were also performed between photosynthetic pigments (Chl_a, Chl_b, $Chl_{a/b}$, Chl_{a+b}, *Car* or Car/Chl_{a+b}) and RGB- or multispectral-derived VIs acquired in Zuera.

Regarding the flammability experiment, we divided the traits under evaluation into two groups: those associated with fuel characteristics (needle length, combustible humidity and fuel bed depth), or *fuel-related* traits, and those associated with flammability characteristics (diffusion flame time, flame time, smoldering combustion time, flame height, fuel combusted and mean peak heat), or *flammability-related* traits. Population differentiation was tested considering *fuel* and *flammability* traits as multidimensional traits through multivariate analysis of variance (MANOVA), and also considering each trait independently through ANOVA, with room temperature and relative humidity used as covariates in the analysis. Statistical analyses were performed using SAS/STAT (Littell et al., 1998).

3. Results

3.1. Intraspecific variability of needle traits

For traits measured *in situ*, only fuel moisture content (*FMC*) of one-year-old needles showed a significant population effect, with populations from the northern Iberian Peninsula and the eastern Mediterranean basin having higher *FMC* than continental and southern Iberian Peninsula populations in July 2nd. The remaining traits did not show significant variability among the subset of populations evaluated in the different sampling campaigns (Table S4).

The mixed models with repeated time structure indicated that all traits varied across sampling dates. However, only *Car* and *FMC* showed significant ($p < 0.05$) and marginally significant ($p < 0.10$) population differentiation, respectively (Table 2). Needle age was significant only for *FMC*, while Chl_a and Chl_{a+b} were significant and marginally significant, respectively, for the interaction between needle age and sampling date (Table 2).

3.2. Relationships between VIs and traits measured in situ

Chl_a was negatively related to *G%* and *TGI*, and marginally negatively related to *GLI* (Fig. 3). These associations seem counterintuitive, but they can be attributed to the fact that we did not measure pigments in current year needles because these needles were not fully developed yet at the time of sampling. *Car* showed marginally significant negative associations with *G%*, *GLI*, *NDVI* and *CCI*, and Car/Chl_{a+b} was also negatively related to *CCI*, and also marginally related to *NDVI* and *GRVI* (Fig. 3). These findings simply suggest that trees having more carotenoids in needle cohorts of 1-year-old and over had in turn more proportion of senescent needles.

3.3. Differences in growth traits and vegetation indexes

Populations exhibited significant differences for total height at both sites, while no differences were found among populations for crown area (Table S5). Total height showed a significant ecotypic effect in Altura, but not in Zuera. In both cases, the population-nested-to-ecotype term was significant (Table S5).

All RGB-derived VIs (*G%*, *GLI*, *GRVI** and *TGI*) differed significantly among populations in Altura. In turn, all VIs exhibited significant ecotypic differences, and also differences among populations nested to ecotypes (Table 3). In Zuera, on the other hand, only *TGI* showed a marginally significant population effect for the June flight (Table 3). Marginally significant ecotypic differences were found for *TGI* and *GLI* for the June flight (Table 3), and only for *GRVI** across flights (Table 4). Although significant time effects were found for *G%* and *GLI*, none of them showed significant interactions between population (or ecotype) and time (Table 4).

For multispectral-derived VIs, population differentiation was

Table 2
Mixed-effects model analysis of variance with repeated time structure for several needle pigments and fuel moisture content of a subset of six populations of Aleppo pine grown in a common garden in Zuera (Spain). Only fixed effects are reported. Chl_a = Chlorophyll a; Chl_b = Chlorophyll b; $Chl_{a/b}$ = ratio between chlorophyll a and b; Chl_{a+b} = total chlorophyll; *Car* = total carotenoids; Car/Chl_{a+b} = ratio between carotenoids and chlorophyll; *FMC* = fuel moisture content. $P < 0.05$ is indicated with bold characters.

			Chl_a		Chl_b		$Chl_{a/b}$		Chl_{a+b}		*Car*		Car/Chl_{a+b}		*FMC*		
Source of variation	Num df	Den df	F-value	P > F	F-value	P > F	F-value	P > F	F-value	P > F	F-value	P > F	F-value	P > F	Den df	F-value	P > F
Block	2	22	1.58	0.229	0.15	0.864	1.36	0.278	0.51	0.607	2.51	0.104	0.31	0.739	22.0	0.45	0.825
Population (Pop)	5	22	1.9.3	0.131	0.07	0.900	0.38	0.855	1.07	0.405	3.39	**0.020**	0.78	0.573	22.0	2.53	*0.059*
Needle age (NA)	1	22	0.01	0.909	0.62	0.439	0.08	0.780	0.16	0.693	2.47	0.131	1.56	0.225	22.0	288.17	**<0.001**
Pop × NA	5	22	0.74	0.620	0.86	0.520	1.21	0.338	0.25	0.937	1.68	0.271	0.48	0.784	22.0	0.87	0.518
Sampling	3	51	53.87	**<0.001**	59.27	**<0.001**	6.31	**0.001**	85.96	**<0.001**	26.12	**<0.001**	22.98	**<0.001**	26.0	11.33	**<0.001**
Pop × Sampling	15	51	1.31	0.230	0.89	0.575	1.19	0.308	0.94	0.528	1.47	0.154	0.66	0.814	26.0	1.93	*0.086*
NA × Sampling	3	51	3.31	**0.027**	0.24	0.868	0.07	0.975	2.20	*0.099*	1.09	0.363	0.64	0.591	26.0	1.71	0.200
Pop × Sampling × NA	15	51	1.27	0.258	0.86	0.608	1.26	0.261	0.82	0.654	1.19	0.310	0.5	0.931	26.0	1.69	0.138
Mean effect size (Population)			0.473 mg g^{-1}		0.068 mg g^{-1}		0.769 mg g^{-1}		0.595 mg g^{-1}		0.186 mg g^{-1}		0.024		1.9 %		

detected in the case of *NDVI* and *PSRI* in Altura (Table 3). Also, *NDVI*, *PSRI* and *TCARI/OSAVI* showed ecotypic differences, and there were also population differences within ecotypes in the case of *NDVI* and *PSRI* (Table 3). In Zuera, *EVI*, *TCARI* and *TCARI/OSAVI* disclosed population differentiation (Table 3; Table S6). The ecotype term was significant for *NDVI*, *EVI*, *TCARI/OSAVI* (Table 3), and *TCARI* and *OSAVI* (Table S6). A schematic representation of the trials along with an example of spatial variation of VIs (for the case of *NDVI*) are provided in supplementary material (Fig. S1, S2). Results regarding vegetation indexes that provided somewhat redundant information (i.e., *TCARI* or *OSAVI*) or did not display population or ecotypic differentiation are also shown in supplementary material (Table S6).

3.4. Relationships between VIs and climate at the origin of populations

In Altura, all RGB-derived VIs of populations (and also *NDVI*) increased eastward along the Mediterranean basin (i.e., positive relationships between longitude and VIs), while *PSRI* increased westward (i.e., negative relationship between longitude and *PSRI*) (Fig. 4). This suggested that populations from the eastern Mediterranean basin had an earlier phenology (i.e., having earlier needle unfolding or old-needle senescence, or both) than their western counterparts. Moreover, *PSRI* was negatively related to mean annual temperature and showed a positive association with latitude and temperature annual range (Fig. 4). Mean diurnal range and isothermality exhibited negative relationships with *NDVI* (Fig. 4). In addition, all RGB-derived VIs showed negative correlations with isothermality (Fig. 4), suggesting that populations exposed to high temperature evenness at origin showed delayed phenology when grown under mesic climatic conditions (i.e., Altura). Climate variables related to precipitation did not show significant relationships with VIs (Fig. 4). In Zuera, on the other hand, a significant eastward increase was found for *TCARI/OSAVI* and (marginally significant) for *GLI* and *TCARI* (Fig. 4).

3.5. Lack of intraspecific variability for traits obtained in the flammability experiment

Our results did not show any differentiation among populations or ecotypes for the suite of traits obtained in the flammability experiment, neither when analyzed together for fuel traits or flammability traits through MANOVA (Table S7), nor independently through ANOVA (Table S8).

4. Discussion

Aleppo pine is a dominant species in fire-prone habitats of the Mediterranean basin adapted to crown fires. However, intraspecific differences in fire-related traits are still poorly studied (Martín-Sanz et al., 2019), especially those related to early season needle unfolding and old needles senescence (Karavani et al., 2018). The latter leads to about one-third of the canopy (that is, all 3 years-old leaves) being dry just before the peak fire season. This increases the probability of crown fire in Aleppo pine at the onset of the fire season (Balaguer-Romano et al., 2020). Needle phenology (e.g., needle unfolding and senescence) may differ among Aleppo pine populations as a result of different adaptive strategies related to water use (Voltas et al., 2015), growth (Lombardi et al., 2022; Patsiou et al., 2020), or fire (Karavani et al., 2018). Needle senescence affecting the old leaves cohort can be triggered by climate factors, especially drought and nutrient availability, and also by specific growth events as a result of remobilization of nutrients from old to young leaves (Peaucelle et al., 2019; Munné-Bosch & Alegre, 2004).

Here, we applied UAV-derived VIs and *in situ* measurements to assess intraspecific variation in the timing of needle unfolding and senescence of Aleppo pine at the onset of the fire season in a range-wide common garden experiment. This assessment was supplemented by an analysis of

	Chl_a	Chl_b	$Cha_{a/b}$	Chl_{a+b}	Car	Car/Chl_{a+b}	FMC
G%	**-0.54**	-0.09	0.09	-0.44	*-0.49*	-0.32	0.10
GLI	*-0.51*	-0.08	0.11	-0.41	*-0.46*	-0.29	0.06
GRVI*	-0.34	0.05	-0.17	-0.22	-0.26	-0.17	-0.35
TGI	**-0.54**	-0.13	0.32	-0.45	-0.38	-0.17	0.29
NDVI	-0.13	0.31	-0.32	0.06	*-0.51*	*-0.53*	0.02
CCI	-0.09	0.42	-0.30	0.16	*-0.57*	**-0.62**	0.25
PRI	0.22	-0.25	0.38	0.04	0.42	0.41	-0.47
PSRI	0.10	-0.16	0.22	-0.01	0.37	0.33	-0.32
GRVI	-0.15	0.24	-0.35	0.02	-0.45	*-0.46*	-0.19
EVI	-0.16	0.15	-0.23	-0.04	-0.30	-0.28	-0.07
TCARI	-0.23	0.07	-0.16	-0.14	-0.13	0.06	0.03
OSAVI	-0.16	-0.21	-0.27	-0.01	-0.40	-0.39	-0.03
TCARI/OSAVI	-0.17	-0.21	0.12	-0.24	0.36	0.46	0.10

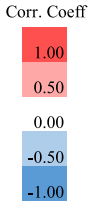


Fig. 3. Pearson correlation coefficients between population means of VIs and several needle pigments or fuel moisture content of a subset of six populations growing in a common garden located in Zuera, eastern Spain. *G%* = green percentage index; *GRVI** = green–red vegetation index; *GLI* = green leaf index; *TGI* = triangular green index; *NDVI* = normalized difference vegetation index; *CCI* = chlorophyll/carotenoid index; *PRI* = photochemical reflectance index; *PSRI* = plant senescence reflectance index; *GRVI* = green ratio vegetation index; *EVI* = enhanced vegetation index; *TCARI* = transformed chlorophyll absorption reflectance index; *OSAVI* = optimized soil adjusted vegetation index. Chl_a = Chlorophyll a; Chl_b = Chlorophyll b; $Chl_{a/b}$ = ratio between chlorophyll a and b; Chl_{a+b} = total chlorophyll; *Car* = total carotenoids; Car/Chl_{a+b} = ratio between carotenoids and chlorophyll; *FMC* = fuel moisture content. $P < 0.05$ is indicated with bold characters.

plastic spatial responses for the same traits by combining results from the Zuera common garden (typical of dry continental conditions) with those of a second, contrasting common garden (representative of a coastal Mediterranean climate).

4.1. Needle traits measured in situ and their relationships with vegetation indexes (VIs)

Most *in situ* measurements related to pigments content as well as the suite of traits related to the litter flammability experiment showed inconclusive patterns regarding intraspecific differentiation. As an exception, population differentiation in early season live fuel moisture content suggests adaptive divergence potentially associated to fire responses. Additionally, the variability in carotenoid content among populations could be related to their different phenological stage or, alternatively, to its photo-protection role under the dry, continental conditions of the trial since our results did not show a clear temporal trend for this pigment indicative of phenological changes. However, these results should be re-examined by securing a larger set of representative populations than the exploratory subset used in this study.

With regard the counterintuitive relationships between needle pigments and RGB-derived VIs, these could have been influenced by the different mixing of needles of different ages among populations (Kuusk et al., 2018). Current-year needles were just emerging at the time of first sampling, and they were not collected for pigments determination; in contrast, the RGB sensor registered reflectance of all needle cohorts. Generally, current-year needles have larger reflections, especially in the green wavelength, as previously reported for other conifers. Therefore, reflectance is likely to decrease with needle age (Hejtmánek et al., 2022; Lhotáková et al., 2021). On the other hand, the relationships between some multispectral indexes (*CCI*, *NDVI*) and the ratio of carotenoids to total chlorophyll content were in line with previous studies conducted in other pine species at their adult (Fréchette et al., 2020, Wong et al, 2019) or seedling stage (D'Odorico et al., 2020). This result points to the existence of population differentiation in pigment contents, especially carotenoids, during the early growing season (Fréchette et al., 2020). It may be related to different intraspecific responses to the onset of summer drought that lead to pre-programmed cell death of old needles or cause changes in photosynthetic phenology, or both (Wong et al., 2020; Peaucelle et al., 2019).

4.2. Do vegetation indexes differ among trials, populations and ecotypes?

Based on the limited time series of VIs available in the continental trial (Zuera), we did not observe obvious temporal patterns which may have differed among populations. However, the ecotypic means of VIs plotted independently for each flight time (May and June) reveal that canopies were in general greener in June, which we interpret as related to the pace of current-year needle development (Fig. 5). On the other hand, we observed higher values of RGB-derived VIs (Fig. 6) and also of NDVI-based VIs (*NDVI*, *EVI*, *TCARI/OSAVI*) and *PSRI* (Fig. 7) in the continental trial (Zuera) than in the coastal trial (Altura). This observation is probably indicating an earlier phenology of trees (i.e., earlier current-year needle unfolding), potentially coupled with an earlier old needle senescence (high *PSRI*), in the continental trial during late spring-early summer. In both trials, the observed population and ecotypic differentiation for many vegetation indexes (i.e., *GLI*, *NDVI*, *TCARI/OSAVI*) suggest variable early season needle phenology related to needle unfolding at the intraspecific level, although with conserved patterns (i.e., similar population plasticity) across sites.

As aforementioned, ecotypes diverged in VIs in a rather consistent manner across trials and suggested that DHT and WST have opposing early season phenology (i.e., timing of needle unfolding and old needle senescence) (Fig. 7). Since variation in needle pigments and water content can be interpreted as differences in the timing of needle unfolding timing among populations in spring (Wong & Gamon, 2015), our results indicate that DHT (an ecotype originating from sub-humid climates) had the earliest phenology (i.e., the earliest needle unfolding) among all ecotypes. This result is in concordance with previous studies pointing to important functional differences among Aleppo pine populations in the same Altura trial (Voltas et al., 2015; Santini et al., 2019a; Lombardi et al., 2021). These studies revealed that drought-sensitive eastern Mediterranean populations (i.e., DHT ecotype) invest comparatively more in aerial growth than in other functional traits such as storage (Santini et al., 2019a), reproduction (Climent et al., 2008) or roots (Lombardi et al., 2021) compared to drought-tolerant western Mediterranean populations (i.e., DSC or DST ecotypes). In turn, they have higher photosynthetic capacity coupled with higher summer

Table 3
Mixed-effects model analysis of variance for RGB and multispectral vegetation indexes of 56 populations of Aleppo pine categorized in five ecotypes and grown in two common gardens (Altura, eastern Spain; Zuera, northeastern Spain). Analysis of variance was fitted independently for each site. Only fixed effects are reported. *G%* = green percentage index; *GRVI** = green–red vegetation index; *GLI* = green leaf index; *TGI* = triangular green index; *NDVI* = normalized difference vegetation index; *PSRI* = plant senescence reflectance index; *EVI* = enhanced vegetation index; *TCARI/OSAVI* = ratio between the transformed chlorophyll absorption reflectance index and the optimized soil adjusted vegetation index. $P < 0.05$ is indicated with bold characters.

				G%		*GLI*		*GRVI**		*TGI*		*NDVI*		*PSRI*		*EVI*		*TCARI/OSAVI*	
Site	Source of variation	Num df	Den df	F-value	P > F	F-value	P > F	F-value	P > F	F-value	P > F	F-value	P > F	F-value	P > F	F-value	P > F	F-value	P > F
Altura	Column	6	18	23.31	**<0.001**	23.06	**<0.001**	9.96	**<0.001**	16.31	**<0.001**	4.20	**0.008**	2.85	**0.039**	14.81	**<0.001**	7.85	**<0.001**
	Block	3	18	4.65	**0.014**	4.47	**0.016**	3.25	**0.046**	2.11	0.134	2.15	0.13	6.25	**0.004**	0.97	0.428	2.22	0.121
	Population	55	112	1.91	**0.002**	1.90	**0.002**	1.93	**0.002**	2.01	**0.001**	1.64	**0.014**	1.92	**0.002**	1.00	0.486	1.28	0.138
	Ecotype	4	100	3.56	**0.009**	3.42	**0.012**	3.27	**0.014**	4.06	**0.004**	3.74	**0.007**	4.07	**0.004**	0.87	0.486	2.64	**0.038**
	Population [Ecotype]	47	100	1.72	**0.012**	1.72	**0.012**	1.79	**0.008**	1.81	**0.007**	1.49	**0.05**	1.80	**0.007**	1.12	0.310	1.33	0.120
	Mean effect size (Population)			0.004		0.008		0.002		0.675		0.014		0.005		0.024			0.015
Zuera	Column	6	18	3.15	**0.027**	3.40	**0.02**	1.45	0.252	5.00	**0.004**	1.55	0.218	0.36	0.892	0.40	0.872	1.02	0.442
	Block	3	18	8.77	**0.001**	4.97	**0.011**	9.67	**0.001**	3.87	**0.027**	1.75	0.193	1.08	0.381	0.99	0.42	0.71	0.558
	Population	55	112	1.16	0.254	1.14	0.278	1.25	0.161	1.36	0.086	1.09	0.35	1.10	0.332	1.62	**0.017**	1.92	**0.002**
	Ecotype	4	100	1.81	0.132	2.36	0.058	1.80	0.135	2.97	**0.023**	2.59	**0.041**	1.05	0.386	3.73	**0.007**	6.13	**<0.001**
	Population [Ecotype]	47	100	1.16	0.266	1.08	0.363	1.28	0.154	1.29	0.148	0.92	0.624	0.98	0.525	1.58	**0.029**	1.74	**0.011**
	Mean effect size (Population)			0.003		0.006		0.003		0.543		0.011		0.005		0.050	0.014		

transpiration than its western counterparts (Santini et al., 2019b). The early needle unfolding of DHT may partly be related to both its high growth plasticity (Lombardi et al., 2022; Patsiou et al., 2020) and its ability to grow well under different climates (Patsiou et al., 2020). It has been shown that populations belonging to this ecotype invest more in aerial growth than in other functional traits such as storage (Santini et al., 2019a), reproduction (Climent et al., 2008) or roots (Lombardi et al.,2021).

While DHT and WST showed the most contrasting differences for all VIs, ecotypes DST and DSC performed generally closer to WST, and ecotype WHC closer to DHT (Figs. 6 and 7). The observation that DHT showed an earlier phenology compared with semi-arid ecotypes probably indicates the existence of adaptive responses linked to a more conservative strategy of populations from drought-prone environments (e.g., higher water-use efficiency, higher root investment), as previously reported for the species (Voltas et al., 2015).

In addition, our findings disclosed ecotypic differentiation in old needle senescence not previously reported for this species, although such differences were clearest in the coastal trial. While WST showed delayed senescence (i.e., low *PSRI*), other semi-arid ecotypes (DSC, DST) showed an opposite pattern (Fig. 7). This observation may effectively indicate changes in early season needle phenology of ecotypes, in particular WST (with a delayed phenology and, thus, later needle development and old needle senescence) and DHT (with an earlier phenology and, thus, earlier needle unfolding and old needle senescence). It may also reflect adaptive differentiation to fire-prone habitats and a trade-off between fire- and drought-related traits, since old needle senescence may be triggered under drought conditions but together it can favor crown fires. This could be the case of ecotypes DST and DSC, which showed late needle unfolding but early old needle senescence (i.e., high *PSRI*), the latter probably triggered by the beginning of the summer drought period (Grulke et al., 2020). The existence of such intraspecific differentiation may be related to the strategy adopted by different populations as driven by their local fire regime, in the same way as other fire-related traits like cone serotiny that has been suggested to be modulated by fire and, indeed, increases its expression under intense fire regimes (Romero et al., 2023). However, this conclusion should be taken with caution, and particularly so since our flammability experiment suggested lack of genetic differentiation in litter flammability traits.

The relationships found between height growth and VIs corroborated the findings above, in particular those involving needle development (i.e., earlier current-year needle unfolding related to enhanced growth). These relationships were partially described by Santini et al. (2019b) for Aleppo pine, particularly the association between aerial growth (volume over bark) and *NDVI*-related indexes, which is primarily linked to differences in total leaf area.

Finally, our results revealed few conclusive associations between climate factors at origin of populations and VIs. In the coastal trial, where climate is wetter, temperature-related factors at origin were the main drivers of population differentiation in VIs. Under these conditions, we could detect a clear longitudinal pattern that indicates earlier needle phenology for populations from the eastern Mediterranean basin compared with their western counterparts. On the other hand, we did not find a clear climatic pattern in the continental trial.

4.3. Methodological limitations

A main limitation of this study is the lack of a complete time series fully covering the onset of the growing season. Instead, we performed two flights spaced one month in late spring (May-June) in the same common garden experiment and, unfortunately, we could only use a single flight (June) for obtaining multispectral VIs due to technical reasons. A higher frequency of flights could definitely improve the characterization of phenological changes in the canopy and, eventually, unveil population or ecotypic differences which may have gone

Table 4
Mixed-effects model analysis of variance for RGB and multispectral vegetation indexes of 56 populations of Aleppo pine categorized in five ecotypes and grown in a common garden located in Zuera (northeastern Spain). Analysis of variance was fitted for a time series comprising two consecutive UAV flights (May and June). Only fixed effects are reported. *G%* = green percentage index; *GRVI** = green–red vegetation index; *GLI* = green leaf index; *TGI* = triangular green index. $P < 0.05$ is indicated with bold characters.

			G%		*GLI*		*GRVI**		*TGI*	
Source of variation	Num df	Den df	F-value	P > F	F-value	P > F	F-value	P > F	F-value	P > F
Column	6	18	3.64	**0.015**	3.46	**0.019**	2.15	**0.097**	7.04	**0.001**
Block	3	18	1.49	0.250	0.68	0.573	2.12	0.133	1.33	0.295
Population (Pop)	55	112	1.44	0.055	1.26	0.153	1.02	0.455	1.44	0.054
Ecotype	4	100	1.78	0.140	1.61	0.178	3.05	**0.021**	1.59	0.182
Time	1	155	658.61	**<0.001**	571.21	**<0.001**	0.93	0.336	1.15	0.286
Ecotype × Time	4	155	0.34	0.847	0.60	0.666	0.83	0.506	0.47	0.757
Pop[Ecotype]	47	100	1.28	0.153	1.33	0.117	1.19	0.230	1.52	**0.041**
Time × Pop[Ecotype]	47	155	0.47	0.998	0.50	0.997	0.70	0.921	0.52	0.995
Mean effect size (Population)			0.003		0.005		0.094		0.524	

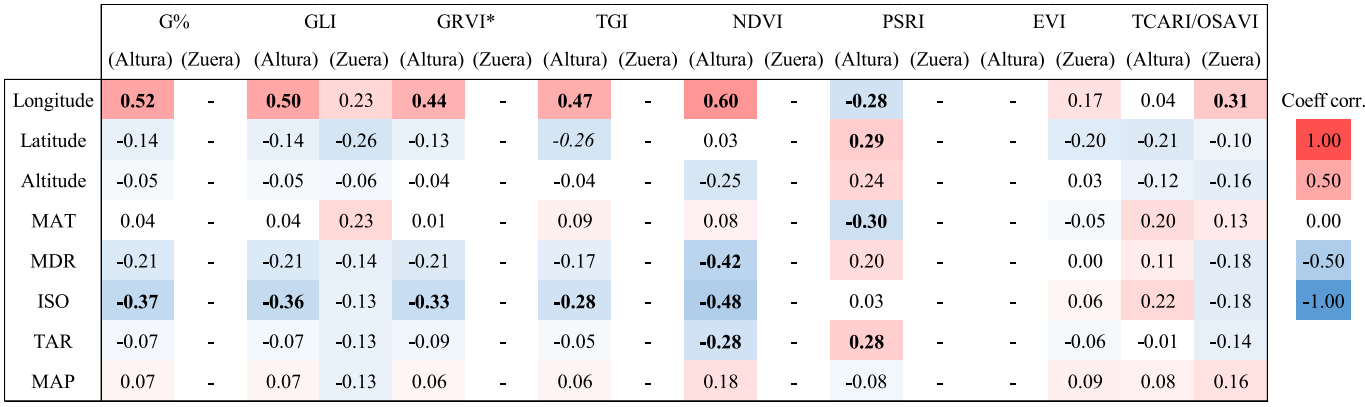


Fig. 4. Pearson correlation coefficients between population means of VIs and climate variables at origin of 56 populations growing in two common garden experiments located in Zuera (northeastern Spain) and Altura (eastern Spain). *GLI* = green leaf index; *TGI* = triangular green index; *PSRI* = plant senescence reflectance index; *EVI* = enhanced vegetation index; *TCARI/OSAVI* = ratio between the transformed chlorophyll absorption reflectance index and the optimized soil adjusted vegetation index. MAT = mean annual temperature; MDR = mean diurnal range; ISO = isothermality; TAR = temperature annual range; MAP = mean annual precipitation. Significant correlations are indicated in bold ($P < 0.05$).

unnoticed using a two-point series of records.

With regard the array of ground truth measurements, we had availability of a larger time series covering one and a half month; however, we sampled a relatively small subset of populations because of personnel and technical constraints, a typical drawback that hampers conventional ecophysiological studies. As a consequence, the development of current-year needles was likely incompletely captured at the intra-specific level. The alternative target of sampling a larger subset of populations or, even, the entire trial could have increased the scope of inferences by disclosing additional patterns of intraspecific differentiation. A similar flaw applies to the litter flammability experiment.

On a separate issue, and regarding both ground measurements and UAV-derived data, the lack of a time series covering multiple years (instead of a single year) also prevented a more complete characterization of genetic patterns. Indeed, a multiyear time-series of records would be desirable to test for consistency of phenological variability across populations and ecotypes of the species. Finally, although previous studies carried out in the Altura trial have revealed important intraspecific differences in Aleppo pine, the joint characterization of functional traits characterizing drought responses across trials (in addition to needle phenology and senescence) would add relevant information about such differentiation and its plasticity, especially regarding the issue of a potential trade-off between fire resistance and drought tolerance.

5 Conclusions

This study showcases the existence of intraspecific variation in needle unfolding and old needle senescence in *P. halepensis*. In turn, this variability is informative of differential plasticity and local adaptation to contrasting conditions across the Mediterranean basin. We found that ecotypes DHT (exposed to dry summers, but with a sub-humid, temperate climate) and WST (with wet summers, but with a semiarid, temperate climate) exhibited the most obvious differences in VIs. Also, ecotypes with semiarid climates shared, in general, similar traits to WST. These findings are likely a result of different life-history strategies and, eventually, trade-offs between fire- and drought-related traits, as exemplified by ecotypes DST and DSC which seemingly exhibited an early old needle senescence coupled with late needle unfolding. On the other hand, the lack of population differentiation for flammability traits suggested similar adaptations to fire for *P. halepensis*. This study represents a first attempt to understand changes in early season needle unfolding and old needle senescence using UAV-derived RGB and multispectral VIs in common garden experiments of adult individuals for a widespread conifer. Our results point to the importance of taking into account the intraspecific characteristics of this species in forest management actions. Particularly, populations (or ecotypes) with high growth potential show increased risk of crown flammability at the onset of the fire season in the Mediterranean basin.

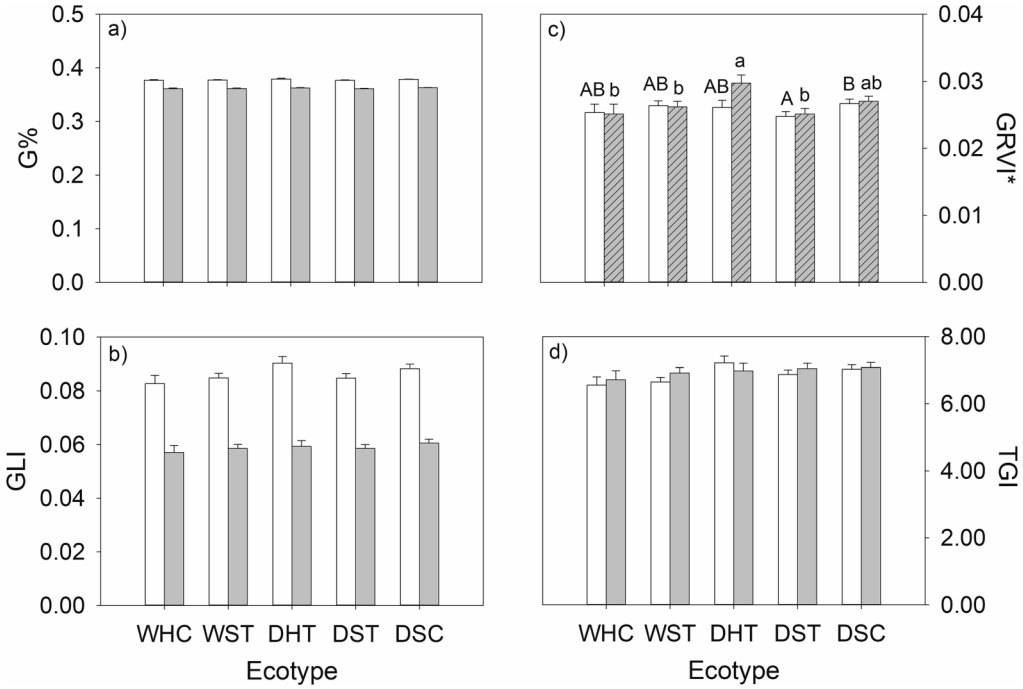


Fig. 5. Barplots summarizing ecotypic differences of RGB- derived vegetation indexes measured in Zuera (northeastern Spain) in two consecutive flights: May (grey bars), June (white bars). Hatched bars denote significant ecotypic differences within a flight and different letters indicate significantly different ecotypes (uppercase letters for June, lowercase letters for May) (LSD test, $P = 0.05$). *G%* = green percentage index; *GRVI** = green–red vegetation index; *GLI* = green leaf index; *TGI* = triangular green index.

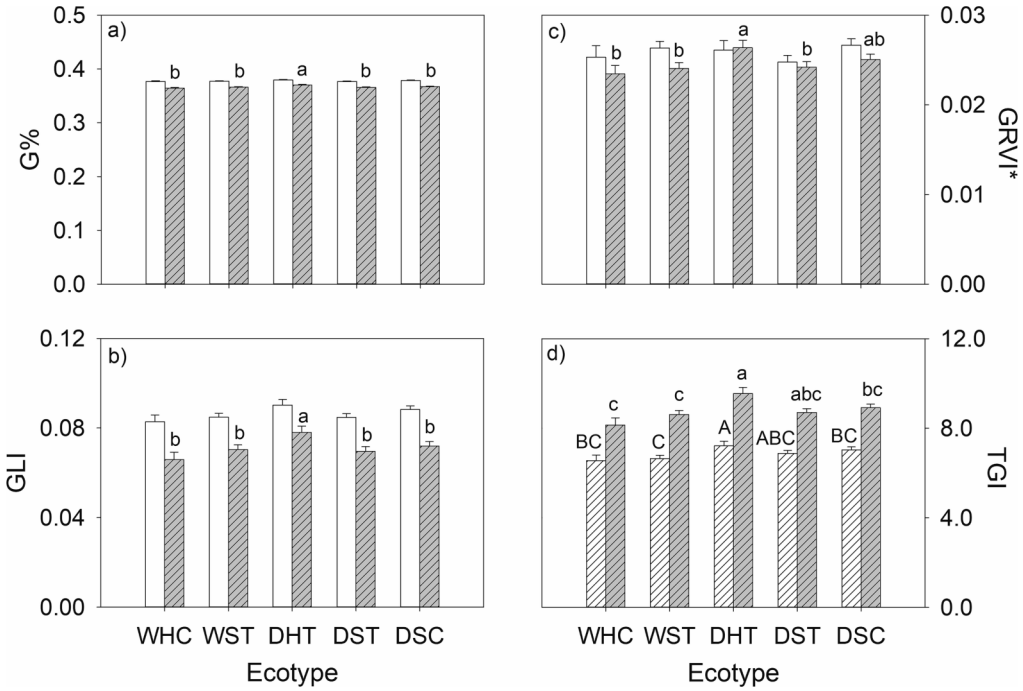


Fig. 6. Barplots summarizing ecotypic differences of RGB- derived vegetation indexes measured in two common garden trials: Altura, eastern Spain (grey bars), and Zuera, northeastern Spain (white bars). Hatched bars denote significant ecotypic differences within trial and different letters indicate significantly different ecotypes (uppercase letters for Zuera, lowercase letters for Altura) (LSD test, $P = 0.05$). *G%* = green percentage index; *GLI* = green leaf index; *GRVI** = green–red vegetation index; *GLI* = green leaf index; TGI = triangular green index.

Data Availability Statement

The data supporting the results of this study will be made available at the CORA open repository (https://dataverse.csuc.cat/) upon acceptance of this article

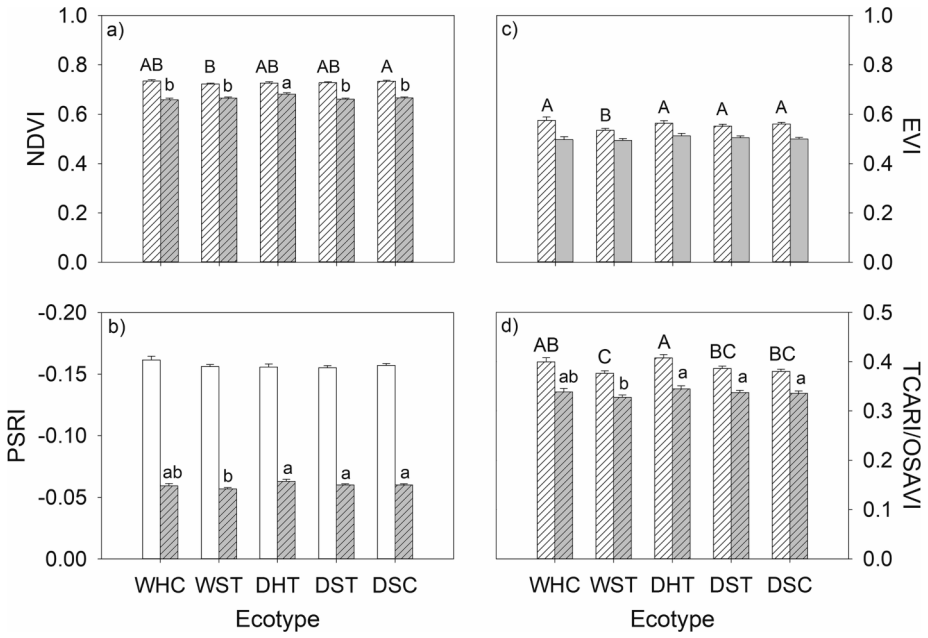


Fig. 7. Bar plots summarizing ecotypic differences of multispectral-derived vegetation indexes measured in two common garden trials: Altura, eastern Spain (grey bars), and Zuera, northeastern Spain (white bars). Hatched bars denote significant ecotypic differences within a trial and different letters indicate significantly different ecotypes (uppercase letters for Zuera, lowercase letters for Altura) (LSD test, $P = 0.05$). *NDVI* = normalized difference vegetation index; *PSRI* = plant senescence reflectance index; *EVI* = enhanced vegetation index; *TCARI/OSAVI* = ratio between the transformed chlorophyll absorption reflectance index and the optimized soil adjusted vegetation index.

CRediT authorship contribution statement

Erica Lombardi: Conceptualization, Methodology, Formal analysis, Data curation, Investigation, Writing – original draft. **Shawn Carlisle Kefauver:** Methodology, Formal analysis, Data curation, Investigation, Writing – review & editing. **Luis Serrano:** Investigation, Writing – review & editing. **Ester Sin:** Investigation, Writing – review & editing. **Paula Piñas-Bonilla:** Investigation, Writing – review & editing. **Beatriz Pérez:** Investigation, Writing – review & editing. **Belén Luna:** Investigation, Writing – review & editing. **Gonzalo Zavala:** Investigation, Writing – review & editing. **Víctor Resco de Dios:** Conceptualization, Supervision, Funding acquisition, Writing – review & editing. **Jordi Voltas:** Conceptualization, Formal analysis, Investigation, Resources, Supervision, Funding acquisition, Writing – review & editing.

Declaration of competing interest

The authors declare that they have no known competing financial interests or personal relationships that could have appeared to influence the work reported in this paper.

Data availability

Data will be made available on request.

Acknowledgments

We would like to thank Javier Madrigal (CIFOR-INIA) for his assistance regarding the flammability protocol and Maria Josep Pau for technical assistance.

Funding

This work was funded by the Spanish Government, grant numbers RTI2018-094691-B-C31 and PID2022-140521OB-C33 (MCIU/AEI/FEDER, EU). E. Lombardi was supported by a AGAUR FI-2022 pre-doctoral fellowship (with the support from the Secretariat for Universities and Research of the Ministry of Business and Knowledge of the Government of Catalonia and the European Social Found).

Appendix A. Supplementary data

Supplementary data to this article can be found online at https://doi.org/10.1016/j.foreco.2023.121475.

References

Alberton, B., Almeida, J., Helm, R., Torres, R. da S., Menzel, A., Morellato, L.P.C., 2014. Using phenological cameras to track the green up in a cerrado savanna and its on-the-ground validation. Ecol. Inform. 19, 62–70. https://doi.org/10.1016/j.ecoinf.2013.12.011.

Anderson, H.B., Nilsen, L., Tømmervik, H., Karlsen, S.R., Nagai, S., Cooper, E.J., 2016. Using ordinary digital cameras in place of near-infrared sensors to derive vegetation indices for phenology studies of High Arctic vegetation. Remote Sens. 8, 847. https://doi.org/10.3390/rs8100847.

Balaguer-Romano, R., et al., 2020. Needle senescence affects fire behavior in Aleppo pine (*Pinus halepensis* mill.) stands: a simulation study. Forests 11, 1–14. https://doi.org/10.3390/f11101054.

Bastien, R., Ganteaume, A., 2020. Correction to: does recent fire activity impact fire-related traits of *Pinus halepensis* Mill. and *Pinus sylvestris* L. in the French Mediterranean area? Ann. For. Sci. 77, 1–19. https://doi.org/10.1007/s13595-020-01021-4.

Berra, E.F., Gaulton, R., Barr, S., 2019. Assessing spring phenology of a temperate woodland: a multiscale comparison of ground, unmanned aerial vehicle and Landsat satellite observations. Remote Sens. Environ. 223, 229–242. https://doi.org/10.1016/j.rse.2019.01.010.

Bulut, S., 2023. Machine learning prediction of above-ground biomass in pure Calabrian pine (*Pinus brutia* Ten.) stands of the Mediterranean region, Türkiye. Ecol. Inform. 74, 101951 https://doi.org/10.1016/j.ecoinf.2022.101951.

Camarero, J.J., et al., 2022. Agricultural and Forest Meteorology Decoupled leaf-wood phenology in two pine species from contrasting climates: longer growing seasons do not mean more radial growth. Agr. For. Meteorol. 327, 109223 https://doi.org/10.1016/j.agrformet.2022.109223.

Chambel, M.R., et al. 2013. Mediterranean Pines (*Pinus halepensis* Mill. and *brutia* Ten.). In: Pâques, L. (eds) Forest Tree Breeding in Europe. Managing Forest Ecosystems, Publ. Springer, Dordrecht. 25, pp. 229-265. doi: 10.1007/978-94-007-6146-9_5.

Chen, A., Orlov-Levin, V., Meron, M., 2019. Applying high-resolution visible-channel aerial imaging of crop canopy to precision irrigation management. Agric Water Manag 216, 196–205. https://doi.org/10.1016/j.agwat.2019.02.017.

Ciocîrlan, C., Curtu, A.L., Radu, G.R., 2022. Predicting leaf phenology in forest tree species using UAVs and satellite images: a case study for European beech (*Fagus sylvatica* L.). Remote Sens. 14, 6198. https://doi.org/10.3390/rs14246198.
Climent, J., et al., 2008. To grow or to seed: ecotypic variation in reproductive allocation and cone production by young female Aleppo pine (*Pinus halepensis, Pinaceae*). Am. J. Bot. 95, 833–842. https://doi.org/10.3732/ajb.2007354.
D'Odorico, P., et al., 2020. High-throughput drone-based remote sensing reliably tracks phenology in thousands of conifer seedlings. New Phytol. 226, 1667–1681. https://doi.org/10.1111/nph.16488.
Fady, B., Semerci, H., Vendramin, G.G., 2003. EUFORGEN Technical Guidelines for Genetic Conservation and Use for Aleppo Pine (*Pinus halepensis*) and Brutia Pine (*Pinus brutia*). International Plant Genetic Resources Institute, Rome, Italy.
Fick, S.E., 2017. WorldClim 2: new 1-km spatial resolution climate surfaces for global land areas. Int. J. Climatol. 4315, 4302–4315. https://doi.org/10.1002/joc.5086.
Fonda, R.W., 2001. Burning characteristics of needles from eight pine species. For. Sci. 47, 390–396. https://doi.org/10.1093/forestscience/47.3.390.
Fréchette, E., Chang, C.Y., Ensminger, I., 2016. Methods paper Photoperiod and temperature constraints on the relationship between the photochemical reflectance index and the light use efficiency of photosynthesis in *Pinus strobus*. Tree Physiol. 36, 311–324. https://doi.org/10.1093/treephys/tpv143.
Fréchette, E., Chang, C.Y.Y., Ensminger, I., 2020. Variation in the phenology of photosynthesis among eastern white pine provenances in response to warming. Glob. Chang. Biol. 26, 5217–5234. https://doi.org/10.1111/gcb.15150.
Gamon, J.A., et al., 2016. A remotely sensed pigment index reveals photosynthetic phenology in evergreen conifers. PNAS 113, 13087–13092. https://doi.org/10.1073/pnas.1606162113.
Gamon, J.A., Penuelas, J., Field, C.B., 1992. A narrow-waveband spectral index that tracks diurnal changes in photosynthetic efficiency. Remote Sens. Environ. 41, 35–44. https://doi.org/10.1016/0034-4257(92)90059-S.
Gamon, J.A., Serrano, L., Surfus, J.S., 1997. The photochemical reflectance index: an optical indicator of photosynthetic radiation use efficiency across species, functional types, and nutrient levels. Oecologia 112, 492–501. https://doi.org/10.1007/s004420050337.
Girard, F., et al., 2011. Polycyclism, a fundamental tree growth process, decline with recent climate change: the example of *Pinus halepensis* Mill. in Mediterranean France. Trees - Struct. Funct. 25, 311–322. https://doi.org/10.1007/s00468-010-0507-9.
Gracia-Romero, A., et al., 2018. Phenotyping conservation agriculture management effects on ground and aerial remote sensing assessments of maize hybrids performance in Zimbabwe. Remote Sens. 10, 1–21. https://doi.org/10.3390/rs10020349.
Grime, J.P., 1977. Evidence for the existence of three primary strategies in plants and its relevance to ecological and evolutionary theory. Am. Nat. 111, 1169–1194. https://doi.org/10.1086/283244.
Grulke, N., et al., 2020. Pre-emptive detection of mature pine drought stress using multispectral aerial imagery. Remote Sens. 12, 1–23. https://doi.org/10.3390/rs12142338.
Haboudane, D., et al., 2002. Integrated narrow-band vegetation indices for prediction of crop chlorophyll content for application to precision agriculture. Remote Sens. Environ. 81, 416–426. https://doi.org/10.1016/S0034-4257(02)00018-4.
Hejtmánek, J., Stejskal, J., Čepl, J., Lhotáková, Z., Korecký, J., Krejzková, A., Dvořák, J., Gezan, S.A., 2022. Revealing the complex relationship among hyperspectral reflectance, photosynthetic pigments, and growth in Norway spruce ecotypes. Front. Plant Sci. 13 https://doi.org/10.3389/fpls.2022.721064.
Huete, A., et al., 2002. Overview of the radiometric and biophysical performance of the MODIS vegetation indices. Remote Sens. Environ. 83, 195–213. https://doi.org/10.1016/S0034-4257(02)00096-2.
Huete, A.R., 2012. Vegetation indices, remote sensing and forest monitoring. Geogr. Compass 6 (9), 513–532. https://doi.org/10.1111/j.1749-8198.2012.00507.x.
Hunt, E.R., et al., 2011. Remote sensing leaf chlorophyll content using a visible band index. Agron. J. 103, 1090–1099. https://doi.org/10.2134/agronj2010.0395.
Hunt, E.R., et al., 2012. A visible band index for remote sensing leaf chlorophyll content at the Canopy scale. Int. J. Appl. Earth Obs. Geoinf. 21, 103–112. https://doi.org/10.1016/j.jag.2012.07.020.
John, J.A., Williams, E.R., 1998. t-Latinized designs. Aust. N. Z. J. Stat. 40, 111–118. https://doi.org/10.1111/1467-842X.00012.
Karavani, A., et al., 2018. Fire-induced deforestation in drought-prone Mediterranean forests: drivers and unknowns from leaves to communities. Ecolo. Monogr. 88, 141–169. https://doi.org/10.1002/ecm.1285.
Kefauver, S.C., et al. 2015. RGB picture vegetation indexes for high-throughput phenotyping platforms RGB picture vegetation indexes for high-throughput phenotyping platforms (HTPPs). In Remote sensing for agriculture, ecosystems and hydrology XVII. SPIE conference. doi: 10.1117/12.2195235.
Klein, T., et al., 2013. Differential ecophysiological response of a major Mediterranean pine species across a climatic gradient. Tree Physiol. 33, 26–36. https://doi.org/10.1093/treephys/tps116.
Kleinsmann, J., Verbesselt, J., Kooistra, L., 2023. Monitoring Individual Tree Phenology in a Multi-Species Forest Using High Resolution UAV Images. Remote Sens. (Basel) 15, 3599.
Klosterman, S., et al., 2018. Fine-scale perspectives on landscape phenology from unmanned aerial vehicle (UAV) photography. Agric. For. Meteorol. 248, 397–407. https://doi.org/10.1016/j.agrformet.2017.10.015.
Kumar, M., et al., 2019. PhenoPine: a simulation model to trace the phenological changes in *Pinus roxhburghii* in response to ambient temperature rise. Ecol. Model. 404, 12–20. https://doi.org/10.1016/j.ecolmodel.2019.05.003.
Kuusk, V., Niinemets, Ü., Valladares, F., 2018. Structural controls on photosynthetic capacity through juvenile-to-adult transition and needle ageing in Mediterranean pines. Funct. Ecol. 32, 1479–1491. https://doi.org/10.1111/1365-2435.13087.
Landis, T., 1990. Characteristics of containers for forest nurseries types of containers chemical root pruning conclusions and recommendations literature cited. North 1–39.
Larrinaga, A.R., Brotons, L., 2019. Greenness indices from a low-cost UAV imagery as tools for monitoring post-fire forest recovery. Drones 3, 6.
Lhotáková, Z., Kopačková-Strnadová, V., Oulehle, F., Homolová, L., Neuwirthová, E., Švik, M., Janoutová, R., Albrechtová, J., 2021. Foliage biophysical trait prediction from laboratory spectra in norway spruce is more affected by needle age than by site soil conditions. Remote Sens. 13, 1–24. https://doi.org/10.3390/rs13030391.
Li, X., et al., 2022. Developing a sub-meter phenological spectral feature for mapping poplars and willows in urban environment. ISPRS J. Photogramm. Remote Sens. 193, 77–89. https://doi.org/10.1016/j.isprsjprs.2022.09.002.
Littell, R.C., Henry, P.R., Ammerman, C.B., 1998. Statistical analysis of repeated measures data using SAS procedures. J. Anim. Sci. 76, 1216–1231. https://doi.org/10.2527/1998.7641216x.
Lombardi, E., et al., 2021. Ground-Penetrating Radar as phenotyping tool for characterizing intraspecific variability in root traits of a widespread conifer. Plant Soil 468, 319–336. https://doi.org/10.1007/s11104-021-05135-0.
Lombardi, E., et al., 2022. UAV-LiDAR and RGB imagery reveal large intraspecific variation in tree-level morphometric traits across different pine species evaluated in common gardens. Remote Sens. 14, 1–21. https://doi.org/10.3390/rs14225904.
Loudermilk, E.L., et al., 2022. Vegetation's influence on fire behavior goes beyond just being fuel. Fire Ecol. 18, 1–10. https://doi.org/10.1186/s42408-022-00132-9.
Louhaichi, M., Borman, M.M., Douglas, E.J., 2001. Spatially located platform and aerial photography for documentation of grazing impacts on wheat. Geocarto Int. 16, 65–70. https://doi.org/10.1080/10106040108542184.
Martín-Sanz, R.C., et al., 2019. How does water availability affect the allocation to bark in a Mediterranean conifer? Front. Plant Sci. 10, 1–13. https://doi.org/10.3389/fpls.2019.00607.
Matthews, S., 2010. Effect of drying temperature on fuel moisture content measurements. Int. J. Wildland Fire 19, 800–802. https://doi.org/10.1071/WF08188.
Mauri, A., et al. 2016. *Pinus halepensis* and *Pinus brutia* in Europe: distribution, habitat, usage and threats. In: San-Miguel-Ayanz J, de Rigo D, Caudullo G, Houston Durrant T, Mauri A (Eds.) European Atlas of Forest Tree Species. Publ. Off. EU, Luxembourg, e0166b8.
McGaughey, R.J., 2015. FUSION/LDV: software for LIDAR data analysis and visualization, Version 3.50; US Department of Agriculture, Forest Service. Pacific Northwest Research Station. University of Washington:, Seattle, WA, USA.
Merzlyak, M.N., et al., 1999. Non-destructive optical detection of pigment changes during leaf senescence and fruit ripening. Physiol. Plant. 106, 135–141. https://doi.org/10.1034/j.1399-3054.1999.106119.x.
Meyer, F., Beucher, S., 1990. Morphological segmentation. J. Vis. Comm. Image Represent. 1, 21–46.
Miller, R.G., et al., 2019. Mechanisms of fire seasonality effects on plant populations. Trends Ecol. Evol. 34, 1104–1117. https://doi.org/10.1016/j.tree.2019.07.009.
Minocha, R., et al., 2009. Development of a standardized methodology for quantifying total chlorophyll and carotenoids from foliage of hardwood and conifer tree species. Can. J. For. Res. 39, 849–861. https://doi.org/10.1139/X09-015.
Motohka, T., et al., 2010. Applicability of Green-Red Vegetation Index for remote sensing of vegetation phenology. Remote Sens. 2, 2369–2387. https://doi.org/10.3390/rs2102369.
Munné-Bosch, S., Alegre, L., 2004. Die and let live: leaf senescence contributes to plant survival under drought stress. Funct. Plant Biol. 31, 203–216. https://doi.org/10.1071/FP03236.
Olmo, V., et al., 2021. Use of sentinel-2 satellite data for windthrows monitoring and delimiting: the case of "vaia" storm in friuli venezia Giulia region (north-eastern Italy). Remote Sens. 13, 1530. https://doi.org/10.3390/rs13081530.
Patsiou, T.S., et al., 2020. Intraspecific responses to climate reveal nonintuitive warming impacts on a widespread thermophilic conifer. New Phytol. 228, 525–540. https://doi.org/10.1111/nph.16656.
Pausas, J.G., 2015. Evolutionary fire ecology: lessons learned from pines. Trends Plant Sci. 20, 318–324. https://doi.org/10.1016/j.tplants.2015.03.001.
Peaucelle, M., et al., 2019. Representing explicit budburst and senescence processes for evergreen conifers in global models. Agric. For. Meteorol. 266–267, 97–108. https://doi.org/10.1016/j.agrformet.2018.12.008.
Picornell-Gelabert, L., et al., 2021. Late Holocene Aleppo pine (*Pinus halepensis* Miller) woodlands in Mallorca (Balearic Islands, Western Mediterranean): investigation of their distribution and the role of human management based on anthracological, dendro-anthracological and archaeopalynological data. Quat. Int. 593–594, 346–363. https://doi.org/10.1016/j.quaint.2020.11.006.
Plowright, M.A., 2018. R Package 'ForestTools.' CRAN. Available online: https://github.com/andrew-plowright/ForestTools.
Popescu, S.C., Wynne, R.H., 2004. Seeing the trees in the forest: using Lidar and multispectral data fusion with local filtering and variable window size for estimating tree height. Photogramm. Eng. Remote Sens. 70, 589–604. https://doi.org/10.14358/PERS.70.5.589.
Resco de Dios, V., et al., 2018. A trade-off between embolism resistance and bark thickness in conifers: are drought and fire adaptations antagonistic? Plant Ecol Divers. 11, 253–258. https://doi.org/10.1080/17550874.2018.1504238.
Risberg, L., Granström, A., 2009. The effect of timing of forest fire on phenology and seed production in the fire-dependent herbs *Geranium bohemicum* and *G. lanuginosum* in

Sweden. For. Ecol. Manage. 257, 1725–1731. https://doi.org/10.1016/j.foreco.2009.01.031.
Romero, B., et al., 2023. Fire frequency, as well as stress response and developmental gene control serotiny level variation in a widespread pioneer Mediterranean conifer, *Pinus halepensis*. Ecol. Evol. 13, e9919.
Rondeaux, G., Steven, M., Baret, F., 1996. Optimization of soil-adjusted vegetation indices. Remote Sens. Environ. 107, 95–107. https://doi.org/10.1016/0034-4257(95)00186-7.
Rouse, J.W., et al., 1973. Monitoring vegetation systems in the Great Plains with ERTS. NASA Spec. Publ 351, 309–317.
Santini, F., et al., 2019b. Using unmanned aerial vehicle-based multispectral, RGB and thermal imagery for phenotyping of forest genetic trials: a case study in *Pinus halepensis*. Ann. Appl. Biol. 174, 262–276. https://doi.org/10.1111/aab.12484.
Santini, F., Climent, J.M., Voltas, J., 2019a. Phenotypic integration and life history strategies among populations of *Pinus halepensis*: an insight through structural equation modelling. Ann. Bot. 124, 1161–1171. https://doi.org/10.1093/aob/mcz088.
Schneider, C., Rasband, W., Eliceiri, K., 2012. NIH Image to ImageJ: 25 years of image analysis. Nat. Methods 9, 671–675. https://doi.org/10.1038/nmeth.2089.
Sharma, Y., Ahmed, R., Sajjad, H., 2022. Assessing vegetation condition across topography in Nainital district, India using temperature vegetation dryness index model. Model. Earth Syst. Environ. 8, 2167–2181. https://doi.org/10.1007/s40808-021-01208-2.
Silvério, D.V., et al., 2015. Surface fire drives short-term changes in the vegetative phenology of woody species in a Brazilian savanna. Biota Neotrop. 15, e20140077.
Sonnentag, O., Hufkens, K., Teshera-Sterne, C., Young, A.M., Friedl, M., Braswell, B.H., Milliman, T., O'Keefe, J., Richardson, A.D., 2012. Digital repeat photography for phenological research in forest ecosystems. Agric. For. Meteorol. 152, 159–177. https://doi.org/10.1016/j.agrformet.2011.09.009.
Springer, K.R., Wang, R., Gamon, J.A., 2017. Parallel seasonal patterns of photosynthesis, fluorescence, and reflectance indices in boreal trees. Remote Sens. 9, 1–18. https://doi.org/10.3390/rs9070691.
Sripada, R.P., Heiniger, R.W., White, J.G., Meijer, A.D., 2006. Aerial color infrared photography for determining early in-season nitrogen requirements in corn. Agron. J. 98, 968–977.
Starý, K., et al., 2020. Comparing RGB-based vegetation indices from UAV imageries to estimate hops canopy area. Agron. Res. 18, 2592–2601. https://doi.org/10.15159/AR.20.169.
Stimson, H.C., Breshears, D.D., Ustin, S.L., Kefauver, S.C., 2005. Spectral sensing of foliar water conditions in two co-occurring conifer species: *Pinus edulis* and *Juniperus monosperma*. Remote Sens. Environ. 96, 108–118. https://doi.org/10.1016/j.rse.2004.12.007.
Taïbi, K., et al., 2014. Testing Aleppo pine seed sources response to climate change by using trial sites reflecting future conditions. New For. 45, 603–624. https://doi.org/10.1007/s11056-014-9423-y.
Thapa, S., Garcia Millan, V.E., Eklundh, L., 2021. Assessing forest phenology: a multi-scale comparison of near-surface (UAV, spectral reflectance sensor, phenocam) and satellite (MODIS, sentinel-2) remote sensing. Remote Sens. 13, 1597. https://doi.org/10.3390/rs13081597.
Tucker, C.J., 1979. Red and photographic infrared linear combinations for monitoring vegetation. Remote Sens. Environ. 8, 127–150. https://doi.org/10.1016/0034-4257(79)90013-0.
Varner, J.M., et al., 2022. Understanding flammability and bark thickness in the genus *Pinus* using a phylogenetic approach. Sci. Rep. 12, 1–10. https://doi.org/10.1038/s41598-022-11451-x.
Varner, J.M., et al. 2015. Flammability of litter from southeastern trees: a preliminary assessment. In: Proceedings of the 17th biennial southern silvicultural research conference, e–Gen. Tech. Rep. SRS–203, Asheville, NC.
Voltas, J., et al., 2015. Intraspecific variation in the use of water sources by the circum-Mediterranean conifer *Pinus halepensis*. New Phytol. 208, 1031–1041. https://doi.org/10.1111/nph.13569.
Voltas, J., et al., 2018. Ecotypic variation and stability in growth performance of the thermophilic conifer *Pinus halepensis* across the Mediterranean basin. For. Ecol. Manage. 424, 205–215. https://doi.org/10.1016/j.foreco.2018.04.058.
Woebbecke, D.M., et al., 1995. Color indices for weed identification under various soil, residue, and lighting conditions. Trans. Am. Soc. Agric. Eng. 38, 259–269. https://doi.org/10.13031/2013.27838.
Wong, C.Y.S., et al., 2019. Carotenoid based vegetation indices for accurate monitoring of the phenology of photosynthesis at the leaf-scale in deciduous and evergreen trees. Remote Sens. Environ. 233, 111407 https://doi.org/10.1016/j.rse.2019.111407.
Wong, C.Y.S., et al., 2020. Tracking the phenology of photosynthesis using carotenoid-sensitive and near-infrared reflectance vegetation indices in a temperate evergreen and mixed deciduous forest. New Phytol. 226, 1682–1695. https://doi.org/10.1111/nph.16479.
Wong, C.Y.S., et al., 2022. Remotely sensed carotenoid dynamics improve modelling photosynthetic phenology in conifer and deciduous forests. Agric. For. Meteorol. 321, 108977 https://doi.org/10.1016/j.agrformet.2022.108977.
Wong, C.Y.S., Gamon, J.A., 2015. Three causes of variation in the photochemical reflectance index (PRI) in evergreen conifers. New Phytol. 206, 187–195. https://doi.org/10.1111/nph.13159.
Xue, J., Su, B., 2017. Significant remote sensing vegetation indices: a review of developments and applications. J. Sensors 2017, 1353691. https://doi.org/10.1155/2017/1353691.
Ye, J., Bao, W., Liao, C., Chen, D., Hu, H., 2023. Corn phenology detection using the derivative dynamic time warping method and sentinel-2 time series. Remote Sens. 15 https://doi.org/10.3390/rs15143456.
Zarco-Tejada, P.J., et al., 2004. Hyperspectral indices and model simulation for chlorophyll estimation in open-canopy tree crops. Remote Sens. Environ. 90, 463–476. https://doi.org/10.1016/j.rse.2004.01.017.